THE ASTROPHYSICAL JOURNAL, 332:646–658, 1988 September 15

SLIM ACCRETION DISKS

M. A. ABRAMOWICZ,[1,2] B. CZERNY,[1,3] J. P. LASOTA,[1,4] AND E. SZUSZKIEWICZ[1]

Received 1987 November 16; accepted 1988 February 29

ABSTRACT

We find a new branch of equilibrium solutions for stationary accretion disks around black holes. These solutions correspond to moderately super-Eddington accretion rates. The existence of the new branch is a consequence of an additional cooling due to general relativistic Roche lobe overflow and horizontal advection of heat. On an accretion rate versus surface density plane the new branch forms, together with the two "standard" branches (corresponding to the Shakura-Sunyaev accretion disk models) a characteristically S-shaped curve. This could imply a limit cycle–type behavior for black hole accretion flows with accretion rates close to the Eddington one.

Subject headings: black holes — stars: accretion

I. INTRODUCTION

The most important scale in accretion disk theory is the Eddington accretion rate, $\dot{M}_E = L_E/c^2 = 1.7 \times 10^{17} M/M_\odot$ g s^{-1}. *Thin accretion disks* are consistent with accretion rates $\dot{M} \ll \dot{M}_E$, and *thick accretion disks* with $\dot{M} \gg \dot{M}_E$. We study here *slim accretion disk* models, with accretion rates $\dot{M} \approx \dot{M}_E$. They differ from both thin and thick disks in several astrophysically important respects.

The slim accretion disk models take advantage of simplification due to vertical integration as used for the thin disks, but at the same time they use the correct thick disk approach to the transonic part of the flow. The momentum and energy equations for the slim disk, which we take from Paczyński and Bisnovatyi-Kogan (1981), contain more terms than the standard Shakura-Sunyaev (1973) equations. The additional inertial term, $v_r dv_r/dr$, describing the dynamical importance of the accretion velocity v_r, and the horizontal pressure gradient term, $\rho^{-1} dP/dr$ are included in the momentum equation, while the advective, horizontal heat flux, $v_r T dS/dr$, is added to the energy equation. The remaining equations are the same as the Shakura-Sunyaev ones. The pseudo-Newtonian potential (Paczyński and Wiita 1980) is used to describe the gravitational field of the central black hole. The inner boundary condition uses the fact that there is no viscous torque across the surface of the black hole, while the outer boundary condition states that at large radii the model of the flow agrees closely with that of Shakura and Sunyaev. The equations together with the boundary conditions and the regularity condition at the sonic point define an eigenvalue problem for l_0, the specific angular momentum of matter crossing the horizon of the black hole. We have solved this eigenvalue problem numerically using a modification of the method described by Muchotrzeb and Paczyński (1982).

Our models form a three-parameter family, with dimensionless parameters (α, $\dot{m}$, m). Here $m = M/M_\odot$ and $\dot{m} = \dot{M}/\dot{M}_C$. The accretion rate is scaled in terms of $\dot{M}_C = \dot{M}_E 16$ rather than $\dot{M}_E$, because, for small accretion rates, 1/16 is the efficiency of accretion in the pseudo-Newtonian potential. Therefore the total (radiative) luminosity of the disk, expressed in the Eddington units $L/L_E = \eta \dot{M}/\dot{M}_E$ for small accretion rates is equal $L/L_E = \dot{M}/\dot{M}_C$. Here η is efficiency of accretion. Figure 1 shows the total luminosity for our disk models (*solid line*) in function of the accretion rate. The dashed line represents the rate of energy generation by viscous stresses. The gap between these lines is due to heat lost through the inner disk radius: for higher accretion rates the heat trapped in matter becomes important, and the flow of matter induces nonnegligible advective, horizontal heat flux. Thus, for higher accretion rates efficiency goes down and luminosity increases not in proportion to the accretion rate, but slower (Jaroszyński, Abramowicz, and Paczyński 1980). Smaller efficiency means that the inner radius of the disk goes closer to the black hole.

Sequences of models with different accretion rates, $0.001 < \dot{m} < 50$, and with the two other parameters fixed at $m = 10$ and $\alpha = 10^{-3}$, are shown in Figure 2. The relation between the accretion rate $\dot{M}$ and the surface density Σ at a fixed radius R has a characteristic S-shape with the three branches (lower, middle, and upper) defining three regimes of accretion. On the *lower branch* the gas pressure P_g is greater than the radiation pressure P_r and the opacity is dominated by electron scattering. The cooling is provided by the vertical radiative flux. Accretion is stable against local thermal and viscous perturbations—as indicated by the positive slope of $\dot{M} = \dot{M}(\Sigma)$. On the *middle branch*, the opacity and cooling mechanism are the same as on the lower branch, but $P_g \ll P_r$ here. Accretion is thermally and viscously unstable—as indicated by the negative slope of $\dot{M} = \dot{M}(\Sigma)$. The thermal instability is due to an insufficient dependence of the rate of radiative cooling Q^- on the vertical thickness of the flow H. For radiative cooling $Q^- \approx H$, while for viscous heating $Q^+ \approx H^2$. Thus, overheating causes expansion and expansion overheating and a thermal runaway instability arises (Pringle, Rees, and Pacholczyk, 1973). The general criterion for thermal stability of the Shakura-Sunyaev model is $(\partial \ln Q^+/\partial \ln H)_\Sigma < (\partial \ln Q^-/\partial \ln H)_\Sigma$ which, for this model, is equivalent to $\beta = P_g/(P_g + P_r) > \frac{2}{3}$. On the *upper branch* accretion flows cannot be described by the Shakura-Sunyaev model. Here $P_g \ll P_r$ and the cooling is provided by both vertical radiative flux and horizontal advection. Because for advective cooling $Q^- \approx H^3$, thermal runaway is avoided and the accretion flow is thermally

[1] Scuola Internazionale di Studi Superiori Avanzati, Trieste, Italy.
[2] Institute of Theoretical Physics, University of California, Santa Barbara.
[3] Department of Astronomy, University of Leicester.
[4] Groupe d'Astrophysique Relativiste CNRS, DARC, Observatoire de Paris, Section de Meudon.

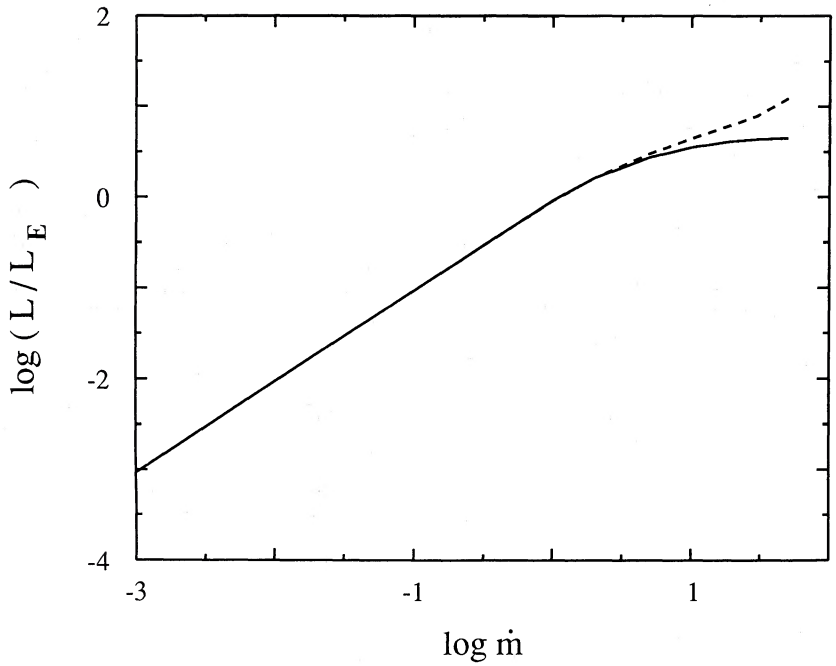

FIG. 1.—The total luminosity for slim disk models (*solid line*) in function of the accretion rate $\dot{m}$. The dashed line represents the rate of energy generation by viscous stresses. $\dot{m}$ is a accretion rate in terms of critical accretion rate, $\dot{M}_C = 64\pi GM/c\kappa_{es}$. All the models are computed with central black hole mass $M = 10M_\odot$, viscosity parameter $\alpha = 0.001$.

stable (Abramowicz 1981). This corresponds to the positive slope of the $\dot{M} = \dot{M}(\Sigma)$ curve.

The existence of the S-shaped $\dot{M} = \dot{M}(\Sigma)$ curves connected with the $\beta > \frac{2}{5}$ instabilities and advective cooling was first suggested in 1985 by Abramowicz and Lasota in an unpublished paper (see also Abramowicz, Lasota, and Xu 1986). The analogy with the dwarf novae case (Smak 1984) is quite appealing. It may indicate the possibility of quasi-periodic outbursts or switching between high and low states for flows with accretion rates which belong to the unstable middle branch of the $\dot{M}(\Sigma)$ curve.

II. BASIC ASSUMPTIONS AND EQUATIONS OF THE MODEL

Paczyński and Bisnovatyi-Kogan (1981) assumed that the vertical thickness of the flow, $H(r)$, is much smaller than the corresponding cylindrical radius, $H/r = \epsilon \ll 1$, and in each

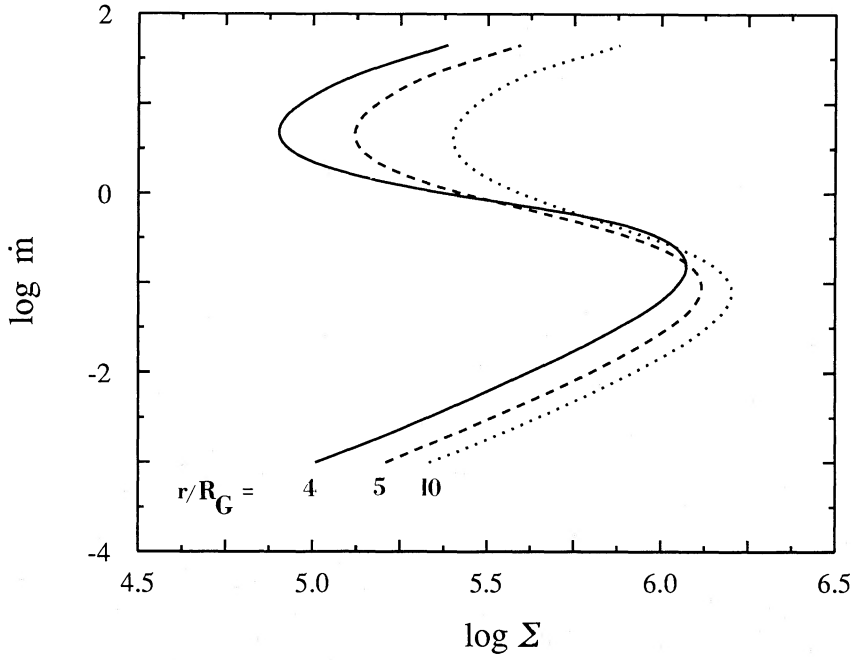

FIG. 2.—The $\dot{m}(\Sigma)$ relation for slim accretion disk models for three fixed radii, $r/R_G = 4$ (*solid line*), 5 (*dashed line*), and 10 (*dotted line*). Σ is a surface density in g cm^{-2}.

equation kept only terms of lowest order in ϵ. For the dimensionless ratios of the horizontal velocity component v_r, and the sound velocity $v_S = (\partial P/\partial\rho)_S^{1/2}$ with the azimuthal velocity component, v_φ, they adopted $v_r/v_\varphi \approx \epsilon^2$ and $v_S/v_\varphi \approx \epsilon$. Because the vertical velocity component v_z is of the order of ϵv_r, they assumed that $v_z = 0$. They also assumed $\partial v_r/\partial z = 0$ and $\partial v_\varphi/\partial z = 0$. Strictly speaking, these assumptions about the velocity field can be made *independently* of the assumption $H/r \ll 1$ and one can obtain consistent physical models with $H/r < 1$. Therefore, the physical validity of the model is *not* directly connected with the small vertical thickness of the flow. However, the numerical method used here works for an accretion rate which is not too high, $\dot{m} < 50$. Numerical difficulties are connected with the radial integral (iteration to get the eigensolution which crosses the critical point); they do not depend on the accuracy of the vertical structure.

If the action of viscosity is due only to shear viscosity and the bulk viscosity can be neglected, the above assumptions assure that the only relevant component of the viscous stress tensor entering the Navier-Stokes equations for the slim disks is

$$\tau_{\varphi r} = \tau_{r\varphi} = \rho\nu\Omega\left(\frac{d\ln\Omega}{d\ln r}\right), \tag{1}$$

where ν is the kinematic coefficient of shear viscosity and $\Omega = v_\varphi/r$ is the angular velocity of rotating matter. According to the Shakura and Sunyaev (1973) viscosity prescription,

$$\tau_{\varphi r} = -\alpha P, \tag{2}$$

where $\alpha = \text{const}$ is a dimensionless, phenomenological viscosity parameter and the pressure is taken at the equatorial plane, $z = 0$. According to equation (2) the viscous torque across a cylindrical surface $r = \text{const}$ is $g(r) = 4\pi r^2\alpha PH$. Using equation (11) this can be written as $g(r) = \dot{M}r(P/\rho)/B_2 v_r$. Because $v_r(R_G) = \infty$, one has $g(R_G) = 0$, i.e., there is no viscous torque across the surface of the black hole. Although this gives no additional restriction, we shall call the fact that $g(R_G) = 0$ *the inner boundary condition.* It will be used later for the integration of the angular momentum balance equation. General relativistic effects are included in our purely Newtonian treatment by using the pseudo-Newtonian potential

$$\Psi = -\frac{GM}{R - R_G}, \tag{3}$$

where $R = (r^2 + z^2)^{1/2}$ and $R_G = 2GM/c^2$ is the gravitational radius of the central black hole which has the mass M. The self-gravity of the accretion disk is totally neglected. The radial component of the gravitational force on the equatorial plane $z = 0$ can be written conveniently as l_K^2/r^3 or $\Omega_K^2 r$, where l_K and Ω_K are the specific angular momentum and angular velocity on Keplerian, circular orbits in the pseudo-Newtonian potential:

$$\Omega_K = \left(\frac{GM}{R^3}\right)^{1/2}\left(1 - \frac{R_G}{R}\right)^{-1} \tag{4}$$

and

$$l_K = (GMR)^{1/2}(1 - R_G/R)^{-1}. \tag{5}$$

The stable Keplerian orbits, with $dl_K/dR > 0$, have radii greater than the radius R_{MS} of the marginally stable orbit located at $R_{MS} = 3R_G$, and the binding energy of the Keplerian orbits, $E_K = \Psi + (\Omega_K l_K)/2$, changes sign at R_{MB}, the radius of the marginally bound orbit. Orbits with radii $R < R_{MB} = 2R_G$ are unbound. The standard equation of state for a mixture of perfect gas and radiation is assumed:

$$P = \frac{\mathscr{R}}{\mu}\rho T + \frac{a}{3}T^4, \tag{6}$$

where μ is the mean molecular weight ($\mu = 0.6$ in what follows). The first law of thermodynamics is used to calculate entropy gradient in terms of density and temperature gradients:

$$TdS = \frac{P}{\rho}\left[\left(12 - \frac{21}{2}\beta\right)\frac{dT}{T} - (4 - \beta)\frac{d\rho}{\rho}\right]. \tag{7}$$

All of the quantities in our model are defined on the equatorial plane. The equations containing only thermodynamical quantities or their functions (equation of state, first law of thermodynamics, viscosity prescription, opacity law) refer to the equatorial plane with no change in form. The same is true for the momentum equations in r and φ directions which contain no z derivatives:

$$\frac{1}{\rho}\frac{dP}{dr} - (\Omega^2 - \Omega_K^2)r + v_r\frac{dv_r}{dr} = 0, \tag{8}$$

and

$$\dot{M}(l - l_0) = g(r) - g(R_G) = 4\pi r^2 H\alpha P. \tag{9}$$

In the derivation of the last equation the inner boundary condition was used. The equation of hydrostatic equilibrium in the z-direction, the continuity equation, and the energy equation, which contain z derivatives, are all integrated vertically. As the vertical disk structure is known only approximately, the results of the integration contain some correcting factors B_i, all of the order of unity. They convert the average vertical values of the z-integrated quantities to their equatorial plane values used in our model. In particular, the equation of hydrostatic equilibrium in the z-direction and the continuity equation read:

$$\Omega_K^2 H^2 = B_1\frac{P}{\rho}, \qquad B_1 = 6 \tag{10}$$

$$\dot{M} = B_2 4\pi r H\rho v_r, \quad B_2 = 0.5, \tag{11}$$

while the energy equation is

$$\dot{M}(l - l_0)\left(-\frac{d\Omega}{dr}\right) + B_3\dot{M}T\frac{dS}{dr} = 4\pi r F^-, \quad B_3 = 0.67. \tag{12}$$

In the energy equation the term connected with the horizontal flux of radiation has been neglected, since it is always much smaller than the other terms and, in particular, much smaller than the vertical radiation flux, F^-:

$$F^- = B_2\frac{c}{\kappa\rho}\frac{aT^4}{3H}. \tag{13}$$

The last formula assumes that the effective optical depth in the vertical direction,

$$\tau_{\text{eff}} = (\kappa_{es}\kappa_{ff})^{1/2}(\Sigma/2) \tag{14}$$

is greater than one, and therefore radiation transfer can be treated in diffusion approximation. Here κ_{es} and κ_{ff} are the electron scattering and free-free opacity coefficients, and $\Sigma = 2H\rho$ is the surface density. In the numerical calculations the opacity coefficient, $\kappa = \kappa(\rho, T)$ was taken from Cox and Stewart (1970).

We have adopted values of B_i from Paczyński and Bisnovatyi-Kogan who estimated them using a polytropic equation of state and averaged, somewhat arbitrarily, the $n = 3$ and $n = 3/2$ cases. The solution depends only very weakly on a particular choice of B_i.

From equations (8) and (11) one gets

$$\frac{d \ln v_r}{d \ln r} = \frac{a_S^2(1 + d \ln H/d \ln r) + v_\varphi^2(1 - \Omega_K^2/\Omega^2)}{v_r^2 - a_S^2} \quad (15)$$

where a_S is a "sound velocity" defined by

$$a_S^2 = \left(\frac{dP}{dr}\right)\left(\frac{d\rho}{dr}\right)^{-1} . \quad (16)$$

Only for isentropic flows is $v_S = a_S$. The numerator and denominator of the right-hand side of equation (15) vanishes at the same *sonic radius* r_S, where

$$v_r^2(r_S) = a_S^2(r_S) , \quad (17)$$

and

$$1 + \left(\frac{d \ln H}{d \ln r}\right)_{rs} = -\frac{v_\varphi^2(r_S)}{a_S^2(r_S)}\left[1 - \frac{\Omega_K^2(r_S)}{\Omega^2(r_S)}\right] . \quad (18)$$

Because $d \ln H/d \ln r > 0$, it follows (Abramowicz and Zurek 1981) that at the sonic radius the angular velocity is *smaller* than the Keplerian value.

III. CONSTRUCTION OF THE MODEL

There are four independent first-order derivatives in the problem: two in equation (8) and two in equation (12). However, the number of independent integration constants which uniquely determine a regular transonic solution is not four, but three, because of an extra algebraic condition (18) at the sonic radius. These three independent integration constants may be connected with the physical conditions at very large radii where we assume that the solution agrees very closely, although not identically, with that of Shakura and Sunyaev. In the Shakura-Sunyaev approximation to the full problem one neglects the horizontal pressure gradient dP/dr and inertial force $v_r\, dv_r/dr$ in equation (8) and the entropy gradient in equation (12). Equation (8) reduces to $l = l_K$ or $\Omega = \Omega_K$. Putting this into the already reduced equation (12) eliminates the last derivative from the problem, which becomes purely algebraic. The location of the inner edge in the Shakura-Sunyaev model is given by $r_{in} = 3R_G$. It is assumed that in this model $g(r_{in}) = 0$. Therefore, the constant $l_0 = l_K(3R_G) = (\frac{3}{2})^{3/2} R_G c$. The algebraic equations which determine the Shakura-Sunyaev solution are nonlinear and we have solved them numerically. However, when the opacity is dominated by electron scattering, i.e., $\kappa(\rho, T) = \kappa_{es} = 0.34$ cm^2 g^{-1} and the total pressure is dominated either by gas, or radiation, the following asymptotic form can be used:

$$P_g \ll P_r: \Sigma[\text{g cm}^{-2}] = 6.232 \mathscr{C}^{-2} \mathscr{R}^{1/2} \mathscr{D} \mathscr{F}^{-1} \alpha^{-1} \dot{m}^{-1} , \quad (19)$$

$$P_g \gg P_r: \Sigma[g \text{ cm}^{-2}] = 3.617 \times 10^5 \mathscr{C}^{-1/5} \mathscr{R}^{-1/5} \mathscr{D}^{-2/5} m^{1/5} \mathscr{F}^{3/5} \alpha^{-4/5} \dot{m}^{3/5} , \quad (20)$$

$$\mathscr{C} = \left(-\frac{d \ln \Omega_K}{d \ln r}\right) , \quad (21)$$

$$\mathscr{R} = \left(\frac{r}{R_G}\right) , \quad (22)$$

$$\mathscr{D} = \left(\frac{r}{R_G} - 1\right) , \quad (23)$$

and

$$\mathscr{F} = \left(1 - \frac{l_K}{l_0}\right) . \quad (24)$$

These formulae provide the Shakura-Sunyaev solution for the surface density Σ in the pseudo-Newtonian potential (see, e.g., Abramowicz 1987). The Shakura-Sunyaev model is artificially singular at $r = 3R_G$. This is caused by incorrect treatment of the flow close to r_{in}, as first noticed by Stoeger (1976). Slim disk models are similar to the thick ones at small radii, and they have no singularities in r_{in}.

Our method of constructing a regular solution with "almost" Shakura-Sunyaev outer boundary conditions follows, with only minor modifications, that of Muchotrzeb and Paczyński (1982). We recall here only the most important features of it, but not the technical details of the numerical code.

First, the values of the central mass M and viscosity parameter α are specified. Next, a value of $\dot{M}$ is chosen, and then, with these values of M, α, $\dot{M}$ we construct the Shakura-Sunyaev solution. This solution is used to determine an initial estimate of the three integration constants needed to start integration from r_{out} downstream. The fourth has already been fixed—it is $\dot{M}$. However, for a *regular* solution, the three integration constants cannot all be given by their Shakura-Sunyaev values, as they are not independent: the regularity condition at the sonic radius (eq. [18]) gives an implicit relation between them which is not known *a priori*. Thus, the initial choice of the three constants must be adjusted, until, for a particular set, a regular transonic solution is found. In the actual numerical procedure instead of adjusting the three outer boundary conditions (i.e., the three integration constants), we change only the integration constant l_0, the angular momentum of matter at the surface of the central black hole. It appears in equation (9) and, as we explained earlier, is the eigenvalue of the problem. The above procedure leaves two unspecified constants in the problem, connected with differences between the functions at the outer radius r_{out} and their Shakura-Sunyaev values. However, the solution at small radii is almost completely insensitive to these remaining degrees of freedom: when the outer boundary conditions are close to the Shakura-Sunyaev ones, the regular transonic solution at small radii is almost *uniquely* determined by M, α, and $\dot{M}$. The value of the outer radius r_{out} where the outer boundary conditions are imposed does not influence the solution at the small radii (Fig. 3).

IV. THE S-CURVES

The most important results found in this paper is the existence, at any fixed radius, of an S-shaped relation $\dot{M}(\Sigma)$. We present this first for a fixed radius, $r = 5R_G$, and then for all radii $r_S < r < r_{out}$. We choose the first particular value of $r = 5R_G$ because most of the heat is produced close to $r = 5R_G$ (see Fig. 12) and therefore this region is most relevant for the observed properties of the disk.

Figure 4 shows the relation between the accretion rate $\dot{M}$ and the surface density Σ at $r = 5R_G$ for models with $\alpha = 0.001$ and $M = 10\, M_\odot$. The solid curve represents our full transonic solution, and the dashed one shows the corresponding Shakura-Sunyaev approximation. The two dotted lines, labeled by (19) and (20), are the analytic asymptotic solutions for radiation-dominated pressure, given by equations (19) and (20). The meaning of the third dotted line, labeled by (29), will be explained later. The two circles show the models computed by Muchotrzeb and Paczyński (1982). The figure quite clearly

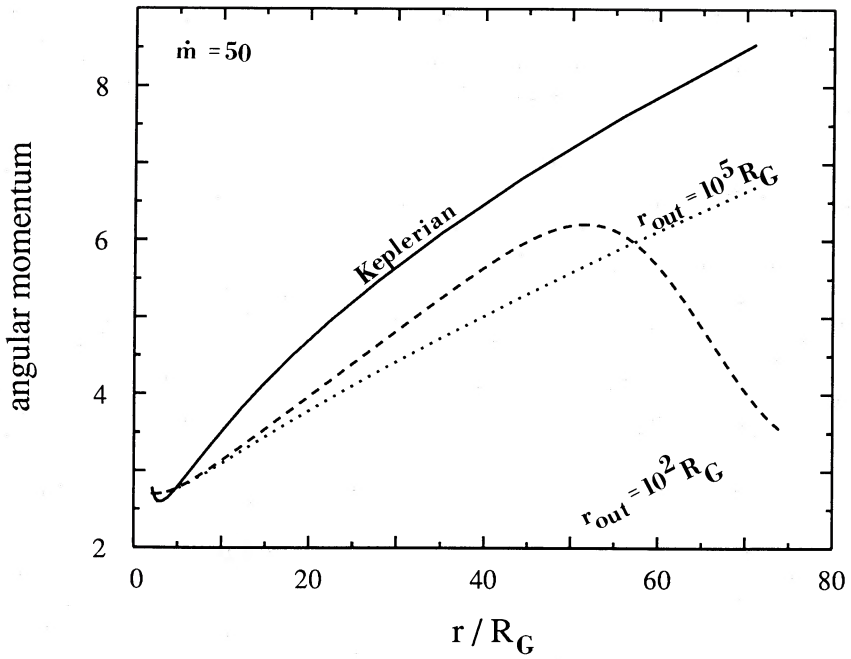

FIG. 3.—The angular momentum distribution for the model with $\dot{m} = 50$ and boundary conditions given in $r_{out} = 10^2 R_G$ (*dashed line*) and $10^5 R_G$ (*dotted line*). Solid line represents the Keplerian angular momentum. Angular momentum is given in $(GMR_G)^{1/2}$.

indicates that both the lower and middle branches of the S-curve are very well described by the Shakura-Sunyaev approximation. Thus the physical properties of the accretion flows belonging to these branches, in particular the stability properties, may be understood in terms of the Shakura-Sunyaev model. Stability properties of the lower and middle branch models have been already summarized in the Introduction. We have recalled there the classical result that the positive slope of the $\dot{M}(\Sigma)$ curve corresponds to stable models and the negative slope—to unstable models. We will not discuss further details of these models here but turn our attention to the upper branch of the S-curve. Obviously this branch cannot be approximated by the Shakura-Sunyaev model.

General relativistic effects in the gravitational field of a black hole, modeled here in terms of the pseudo-Newtonian potential (3), cause a characteristic behavior of the equipotential surfaces

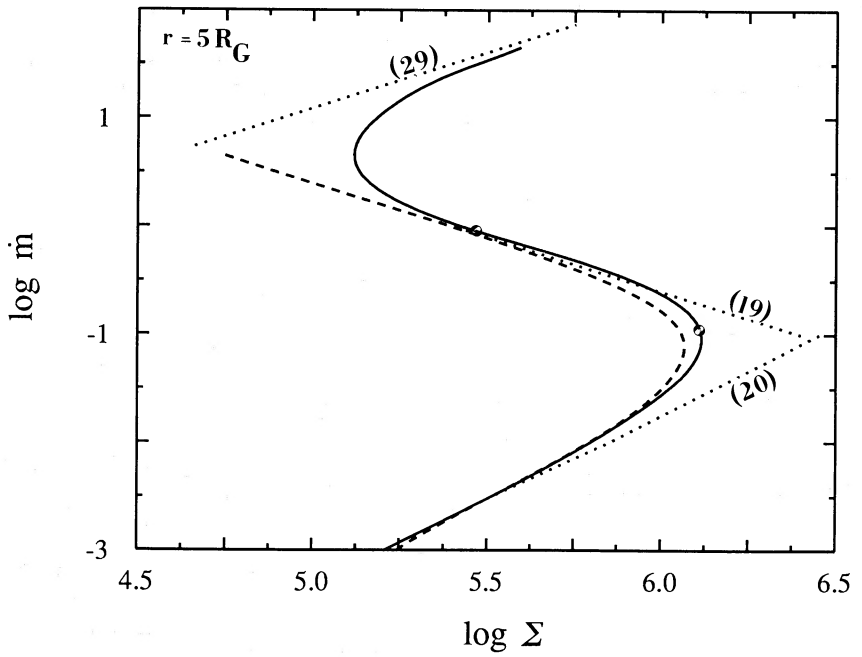

FIG. 4.—The $\dot{m}(\Sigma)$ relation for $r = 5R_G$. Full transonic solution (*solid line*), Shakura-Sunyaev approximation (*dashed line*), analytic asymptotic solutions for gas-dominated (*dotted* [20] *line*) and radiation-dominated pressure (*dotted* [19] *line*), approximation for the upper branch slope (*dotted* [29] *line*).

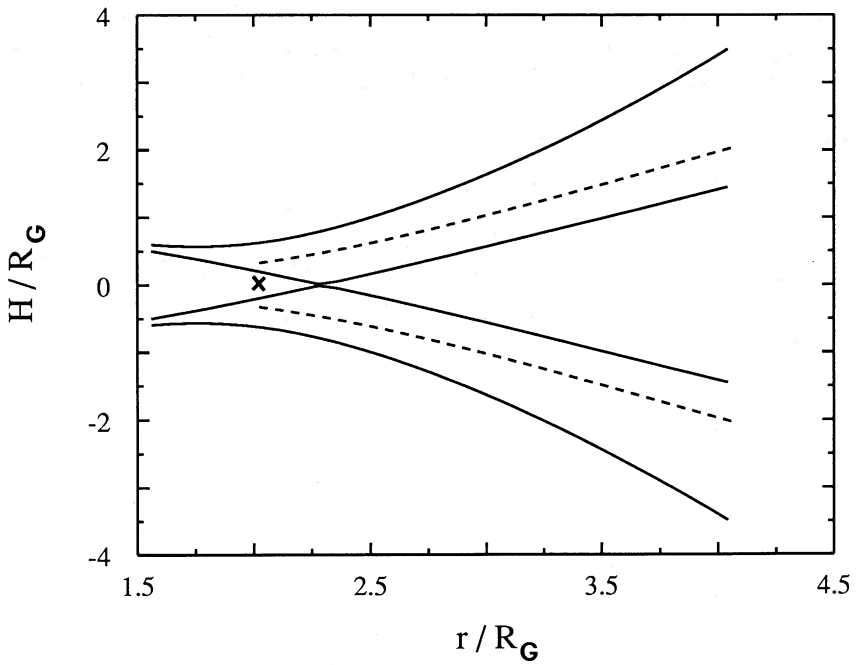

FIG. 5.—The equipotential surfaces (*solid lines*) and the surface of the disk model with $\dot{m} = 10$ (*dashed lines*). Cross indicates the position of the sonic point.

close to the *inner edge* of the disk, defined as the smaller of the two roots of the equation

$$l(r_{\rm in}) = l_{\rm K}(r_{\rm in}) \,. \tag{25}$$

The larger root corresponds to the *physical center* of the disk. On the equipotential surfaces, the total potential (gravitational plus centrifugal), defined by

$$W(r, z) = \Psi(r, z) + \int l^2(r) r^{-3} dr \tag{26}$$

is constant. In Figure 5, the equipotential surfaces (*solid lines*) are shown for a particular model with $\dot{M} = 10\dot{M}_C$. The surface of the disk is marked with dashed lines. The location of the sonic point r_S is indicated by a small cross. Note that $r_S < r_{\rm in}$, in agreement with our comment in connection with equation (18). One of the equipotentials, $W = W_R$, crosses itself at $r = r_{\rm in}$. When $r_{\rm in} < 3R_G$ a characteristic *cusp* is formed at the crossing. If the surface of the disk, $W = W_S$, slightly overflows the critical equipotential $W = W_R$, called *the Roche lobe*, then the mechanical equilibrium is slightly destroyed, causing mass loss, and consequently also a heat loss. The physical picture is analogous to Roche lobe overflow in close binaries. In the case when $r_{\rm in} > 3R_G$, no cusp is formed, and the Roche lobe mechanism does not operate. The heat loss rate close to the cusp has the behavior

$$Q^- \approx H^3 \,. \tag{27}$$

Exact formulae for mass loss and cooling due to the Roche lobe overflow mechanism have been given by Abramowicz (1986), but for our present discussion the approximate version (27) is sufficient. The criterion mentioned in the Introduction for thermal stability of Shakura-Sunyaev disk models states

$$\left(\frac{\partial \ln Q^-}{\partial \ln H}\right)_\Sigma > \left(\frac{\partial \ln Q^+}{\partial \ln H}\right)_\Sigma \,. \tag{28}$$

Because for the standard viscosity law (2) the right-hand side of this inequality is equal to 2, and for Roche lobe overflow cooling the left hand side is equal to 3, according to equation (27), the inequality is fulfilled, which means that the region of the disk cooled by the Roche lobe overflow mechanism is thermally stable.

For small accretion rates the stabilized region lies in the immediate vicinity of the inner edge, but for $\dot{M} \geq \dot{M}_C$ the size of this region is substantially greater, as demonstrated by the following argument. Consider a fluid element located at a distance Δr from the inner edge of the disk, in the unstable part. The element expands vertically in the *thermal* time $t_{\rm th} = 2\pi/\Omega\alpha$ because of the overheating caused by the thermal instability. At the same time it is traveling downward in a radial drift time, $t_{\rm dr}$, which, in the Shakura-Sunyaev model, equals the viscous time, $t_{\rm vis} = t_{\rm th}(H/r)^{-2}$. If the element is able to arrive at $r = r_{\rm in}$ before it expands the distance H, the Roche lobe overflow mechanism will cool the element, and the instability will be surpressed. Therefore, in the stabilized region $t_{\rm vis} \approx t_{\rm th}$, or $H \approx r$. In the above argument the expressions for $t_{\rm th}$ and $t_{\rm vis}$ have been taken from the Shakura-Sunyaev model, which assumes a Keplerian distribution of angular momentum. However, for the disks with sufficiently high accretion rates the angular momentum at small radii is not Keplerian, but almost constant (see Fig. 9). Thus, less viscous reprocessing of the angular momentum is needed and the element travels the distance Δr in a time shorter than $t_{\rm vis}$. This simple argument correctly predicts that the Roche lobe overflow stabilization is important for flows with accretion rates $\dot{M} \approx \dot{M}_C$ or greater, and therefore, that the S-curve should bend at approximately $\dot{M} \approx \dot{M}_C$. The Roche lobe overflow cools down globally the whole innermost part of the disk. Locally, however, at some radius $r < 5R_G$, the advective flux $F_{\rm adv}$ could either cool or heat the flow. At higher accretion rates the advective flux in the more distant parts of the disks is always an important cooling mechanism (Fig. 6). The slope of the upper branch of the

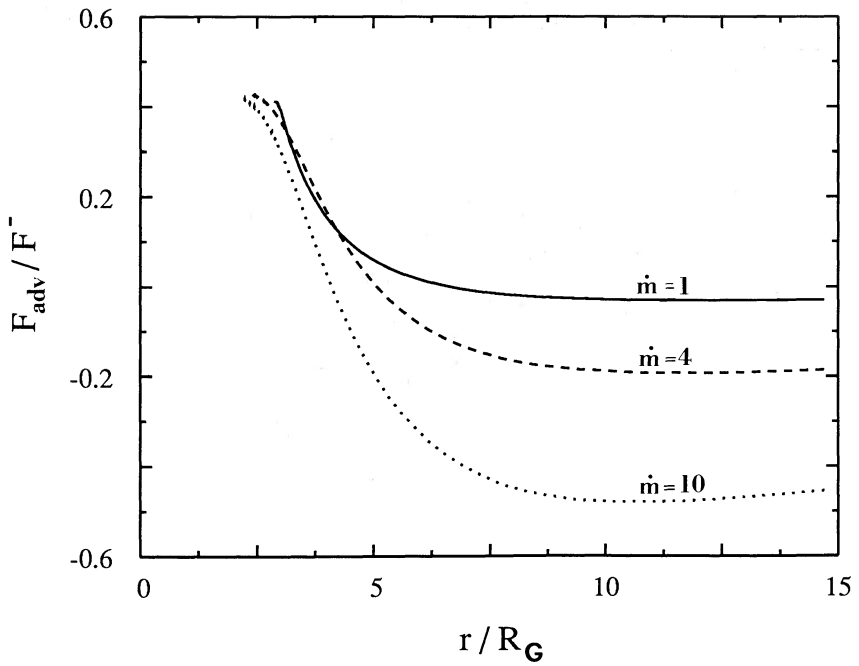

FIG. 6.—The ratio of the advective and radiative fluxes as a function of radius for three accretion rates $\dot{m} = 1$ (*solid line*), 4 (*dashed line*), 10 (*dotted line*)

S-curve can be estimated from an equally simple argument. Assuming that radiation pressure dominates and that the rotation is Keplerian, we replace the entropy gradient term in the energy equation (12) by $8P/r\rho$, using equation (7) and $dS/dr \approx S/r$. All of the equations are now linear algebraic. The solution for the surface density gives $\Sigma = f(r)\alpha^{-1}\dot{M}$, where $f(r)$ is a function of r, known with accuracy up to a constant factor, the value of which is rather poorly estimated in this approximation. However the slope of the $\dot{M}(\Sigma)$ curve on the upper branch is exactly recovered:

$$\ln \Sigma = \text{const} + \ln \dot{m} - \ln \alpha \, . \tag{29}$$

This relation is shown in Figure 4 by the dotted line labeled (29).

At the radius $r = 5R_G$ the accretion rates at the lower (labeled B) and upper (labeled A) turning points of the S-curve are

$$\dot{M}_B(5R_G) = 0.09\dot{M}_C \, , \quad \dot{M}_A(5R_G) = 4.5\dot{M}_C \, . \tag{30}$$

Figure 7 shows the accretion rates at the turning points for different radii (solid lines marked A, B). In the same figure the dashed lines are those of $\beta = \text{const}$. They are labelled by the values of β. The dotted line represents the location of the sonic point in the models with different accretion rates.

With the exception of a small region at $r \approx r_S$ the $\dot{M}_B(r)$ curve agrees with that for $\beta = \frac{2}{5}$ for all r as it should in the Shakura-Sunyaev model. In particular, for $r = 6.4R_G$ it has a minimum

$$\dot{M}_{\min} = 0.1\dot{M}_C \tag{31}$$

predicted by the Shakura-Sunyaev approximation for the $\dot{M}_B(r)$ curve gives an analytic expression (Abramowicz 1987)

$$\dot{m}(r) = 8.796 \times 10^{-4}\mathscr{C}^{-9/8}\mathscr{R}^{7/16}\mathscr{D}^{7/8}\mathscr{F}^{-1}\alpha^{-1/8}m^{-1/8} \, . \tag{32}$$

This diverges at $r = r_{\text{in}} = 3R_G$, but this is an artifact of the Shakura-Sunyaev model, connected with the improper treatment of the flow close to the inner edge. Accretion flows with $\dot{M} < \dot{M}_{\min}$ are everywhere stable against the $\beta < \frac{2}{5}$ instability.

The location of the sonic point changes from the radius of the marginally stable orbit $R_{MS} = 3R_G$ for small accretion rates, to the radius of marginally bound orbit $R_{MB} = 2R_G$ for very high accretion rates. This is a typical behavior for thick accretion disks, which have very low values of $\alpha < 0.001$. (See, e.g., Madau 1988 or Begelman, Blandford, and Rees 1984 for a discussion of the limits on α in thick disks.) Kozłowski, Jaroszyński, and Abramowicz (1978) proved, using an exact analytic method, that for $\alpha = 0$ the inner edge of a thick disk is always located between R_{MS} and R_{MB}, while other authors (e.g., Paczyński 1980 or Różyczka and Muchotrzeb 1982) who used numerical thick disk models with $\alpha \ll 1$ found a behavior similar to that shown in Figure 7. However, for accretion flows with higher values of α the situation is remarkably different. We discuss this point in § VI.

V. DETAILS OF THE SLIM DISK MODELS

Figure 2 in the Introduction shows how the surface density Σ depends on accretion rate for three fixed radii, $r/R_G = 4$, 5, 10. The behavior at other radii is similar.

To discuss other properties of slim disks we have chosen five models with

$$\dot{m} = 0.01, \, 0.1, \, 1, \, 4, \, 10 \, ,$$

located at characteristic points of the S-curve. (The three branches and two turning points). Figure 8 shows how the thickness of the flow depends on radius for these five accretion rates. The initially thin disk ($H/R \ll 1$) becomes thicker with increasing accretion rate but always remains slim, i.e., the assumption $H/R < 1$ is always satisfied.

The question of how to specify the correct boundary conditions at large radii is not an easy one. Figure 9 clearly indicates that with increasing accretion rate the angular momentum

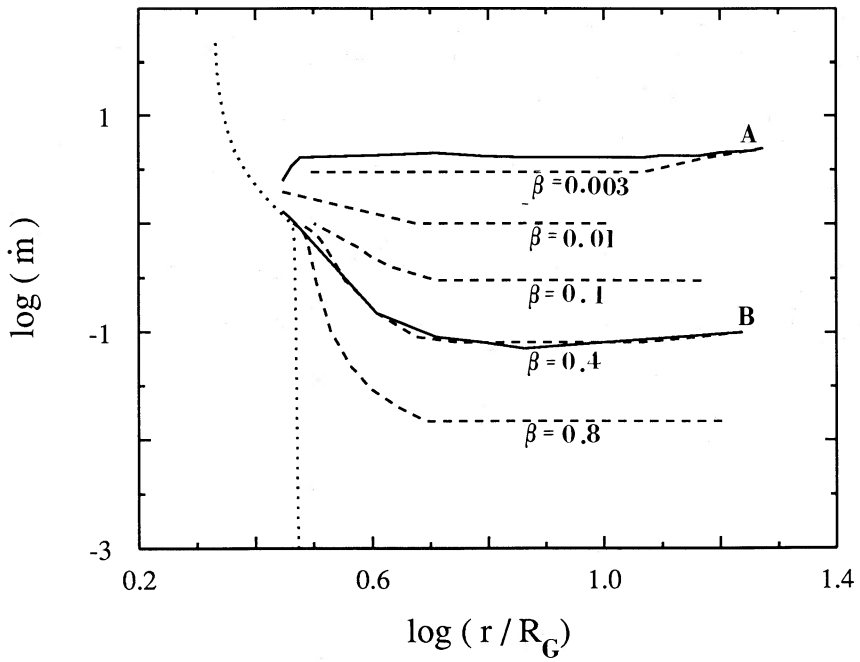

FIG. 7.—The location of the turning points on the S-curves as a function of radius (*solid lines* labeled A and B). The dashed lines indicate the lines of the constant β. The dotted one represents the location of the sonic points.

differs more and more from the Keplerian distribution at both small *and* large radii. The tendency of the angular momentum distribution to become flatter with increasing accretion rate, evident in our numerical models, was found, on general theoretical grounds, by Begelman (1978) in the thick disk case. The agreement suggests a continuous path from slim to thick disks along the sequence of models with increasing accretion rate, correctly placing the slim disks between the thick and thin ones. However, this path cannot be completed in practice with the actual method used in our paper, because the method fails for $\dot{M} > 50\dot{M}_C$.

We have already discussed the meaning and the physical importance of the points r_c and r_{in} at which $l(r)$ crosses the Keplerian distribution, $l_K(r)$. The location of these points, and the value of l_0, the angular momentum of matter at the black hole surface, are all shown in Figure 10 as functions of the accretion rate. For small accretion rates, $l_0 \approx l_{MS}$, and $r_{in} \approx R_{MS} = 3R_G$ as in the standard Shakura-Sunyaev model. The

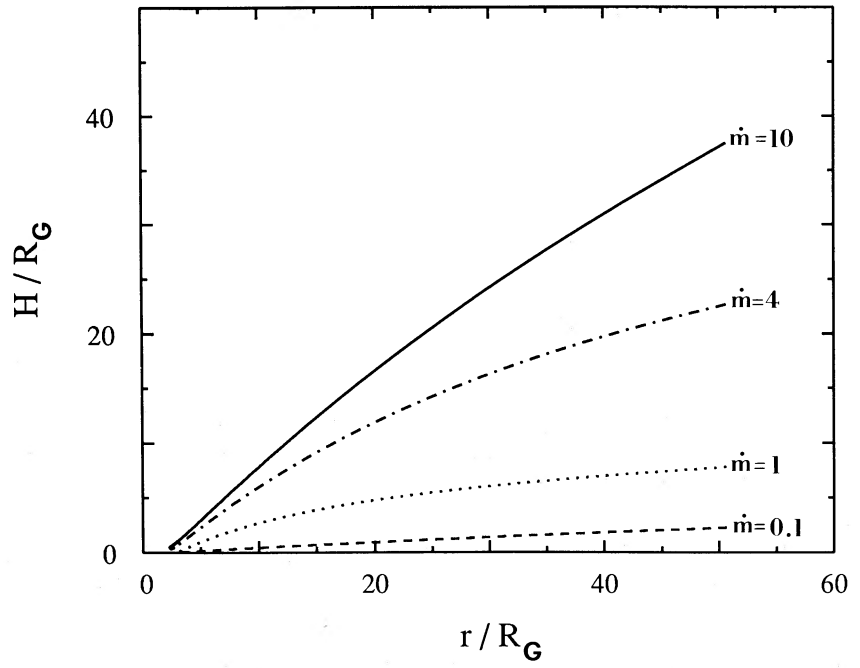

FIG. 8.—The thickness of the flow for the different accretion rates: $\dot{m} = 0.1$ (*dashed line*), 1 (*dotted line*), 4 (*dash-dotted line*), and 10 (*solid line*)

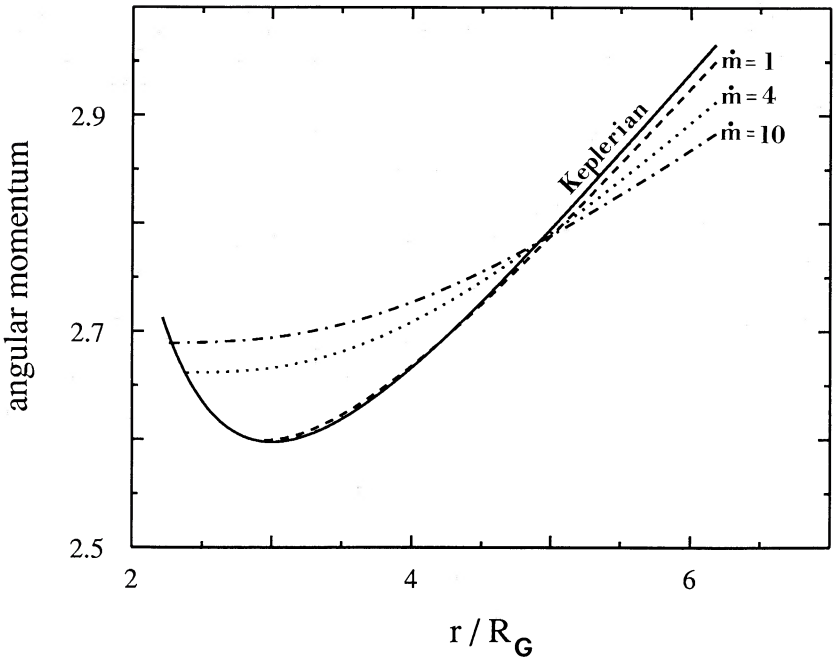

FIG. 9.—The angular momentum distribution for $\dot{m} = 1$ (*dashed line*), 4 (*dotted line*), 10 (*dash-dotted line*), and the Keplerian one (*solid line*)

precise location of r_c for small accretion rates cannot be correctly estimated in the standard model, because it depends critically on the details of heat and angular momentum balance which are not treated properly in this model; the curves $l(r)$ and $l_K(r)$ are almost parallel close to $r = r_c$. For high accretion rates, $r_{in} \approx R_{MB} = 2R_G$ and $l_0 \approx l_{MB}$, in excellent agreement with the thick disk theory. Because, as we have already mentioned, for high accretion rates $l(r) \approx$ const at small radii, from the above described behavior of r_{in} and l_0 it follows that, for high accretion rates, r_c should be $\approx 5R_G$, which can clearly be seen to be the case in our numerical models. Figures 11 and 12 show the variation of temperature with radius and also the closely connected variation of the vertical radiation flux F^-. These curves are very similar to those familiar from the Shakura-Sunyaev models. In particular, the maximum value of the temperature, T_{max} is reached at a small radius, between $4R_G$ and $6R_G$, with the precise value depending on the accretion rate. The function $T_{max}(\dot{M})$ is shown in Figure 13 by the solid line. The Shakura-Sunyaev model predicts $\log T_{max} \approx \frac{1}{4} \log \dot{M}$. Our models were con-

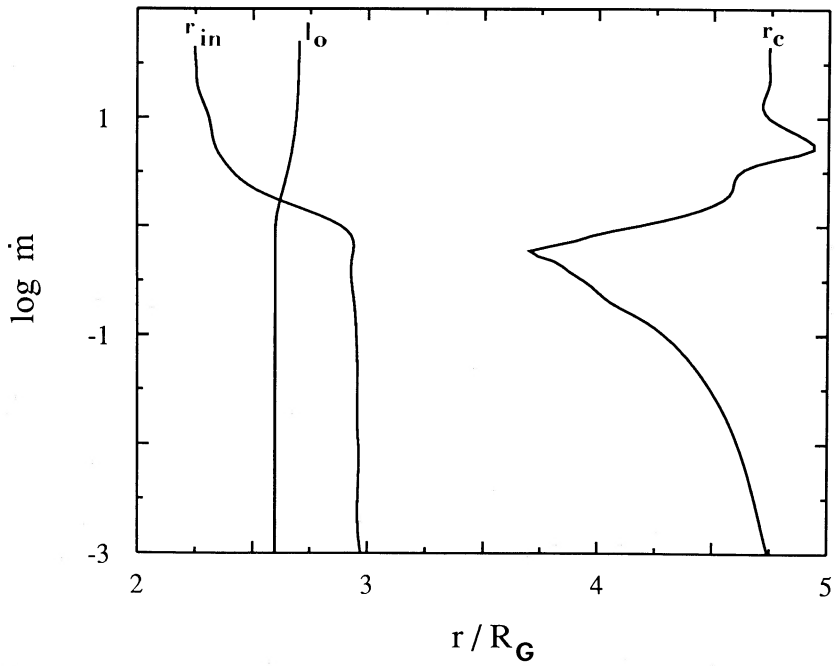

FIG. 10.—The location of r_{in}, r_c, and l_0 as a function of accretion rate

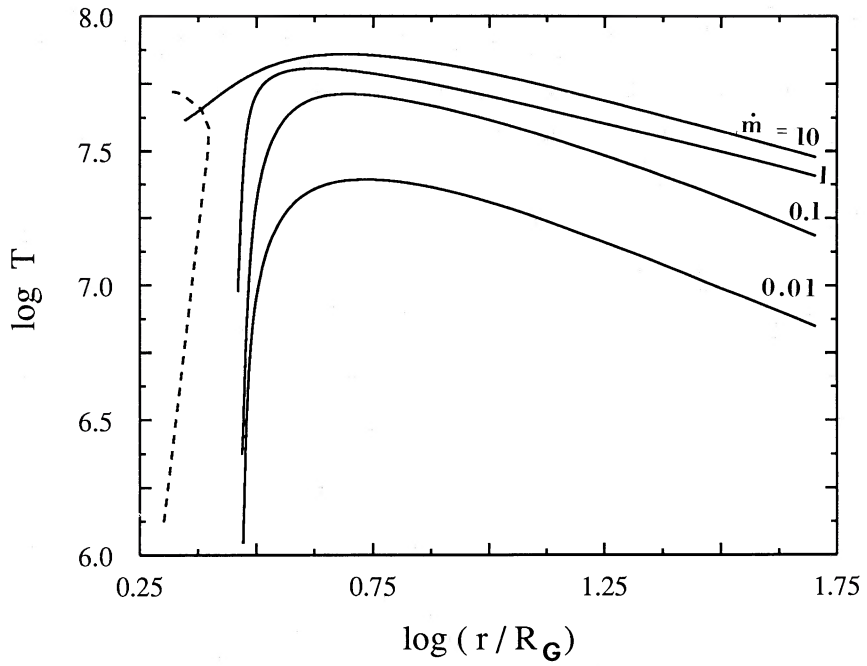

FIG. 11.—The temperature distribution for models with $\dot{m} = 0.01, 0.1, 1$, and 10. The boundary of a region where $\tau_{\rm eff} < 1$ is shown by the dashed line.

structed for $\tau_{\rm eff} > 1$; cf. equation (14). This condition was always checked *a posteriori*, and it was found to be true almost everywhere in all the models, with exception of a small region shown in Figure 11 (left from the dashed line).

VI. DISCUSSION

In this section we discuss only the assumption about the magnitude and form of the viscosity, because only this assumption is really restrictive. Modificiations of it introduce *qualitative* changes in the physical properties of the models. The other assumptions and approximations are relevant for accuracy, but not for physics.

a) The Magnitude of α in Shakura-Sunyaev Viscosity Prescription (2)

The fact that transonic accretion flows with small and large α are qualitatively different was noticed by Muchotrzeb (1983) and has been discussed by many authors (e.g., Matsumoto *et al.* 1984). In Figure 14 we show the location of the sonic point as a function of the accretion rate for $\alpha = 10^{-4}$,

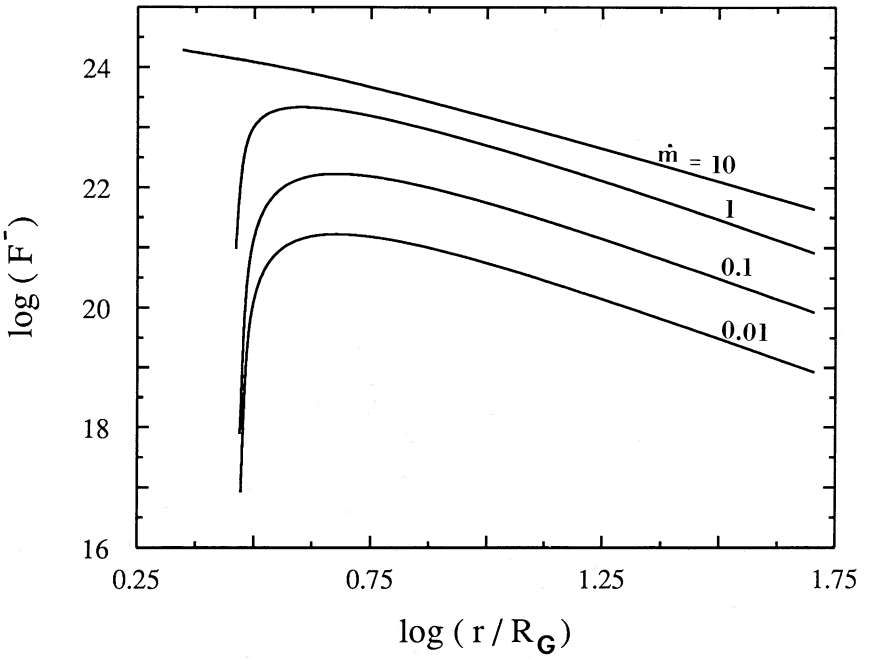

FIG. 12.—The radiative flux from the disk surface as a function of radius for $\dot{m} = 0.01, 0.1, 1$, and 10

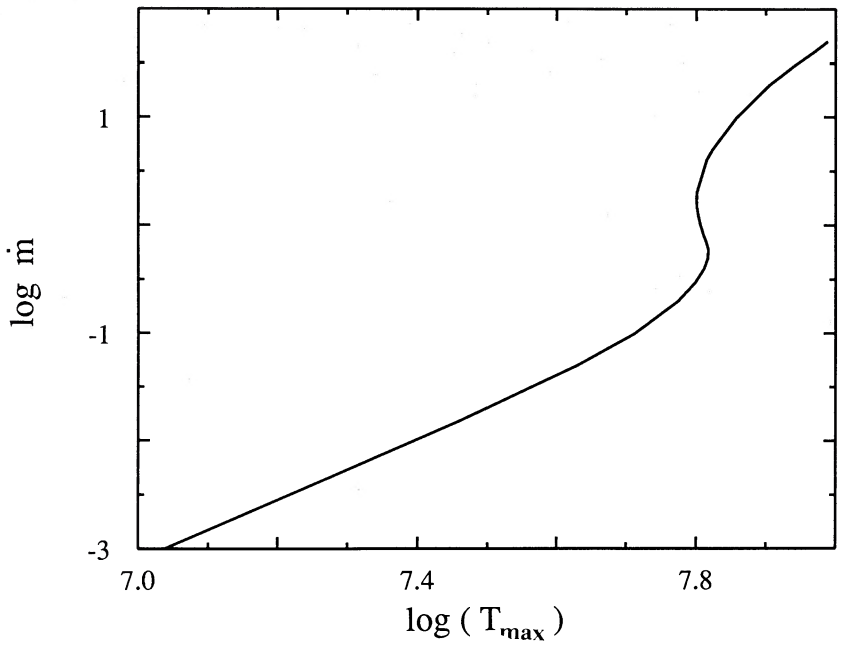

FIG. 13.—The accretion rate–maximum temperature relation

5×10^{-2}, 10^{-1}, and 0.5. Feed small α, equal to 10^{-4}, the typical behavior for the thick accretion disks is evident: with increasing accretion rate, the sonic point moves from R_{MS} toward R_{MB} (cf. Paczyński 1980 and Różyczka and Muchotrzeb 1982). For the highest value of α, equal to 0.5. the sonic point moves with increasing accretion rate in the opposite direction, while for the intermediate value, $\alpha = 10^{-1}$, the behavior is more complicated, but for both small and large accretion rates it is similar to that for $\alpha = 0.5$. The physical reason for these two different behaviors is explained in Figure 15 which compares the Keplerian angular momentum distribution (*dotted line*) with the distributions in two accretion disk models (*solid lines*): one with small $\alpha = 0.001$ and the other with high $\alpha = 1$. In the low viscosity case, the $l(r)$ curve crosses the Keplerian one in two points corresponding to the physical center r_c and the inner edge r_{in} of the disk (in addition $r_{in} < 3G_G$). It is well known from the thick accretion disk theory (e.g., Abramowicz, Calvani, and Nobili 1980) that in this case the Roche lobe overflow mechanism operates at $r = r_{in}$. Accretion onto the central object is due to a slight violation of mechanical equilibrium and needs no help from viscosity. In the high-viscosity case, the angular momentum is everywhere sub-Keplerian, the Roche lobe overflow mechanism does not operate, and accretion is due only to viscous processes. The

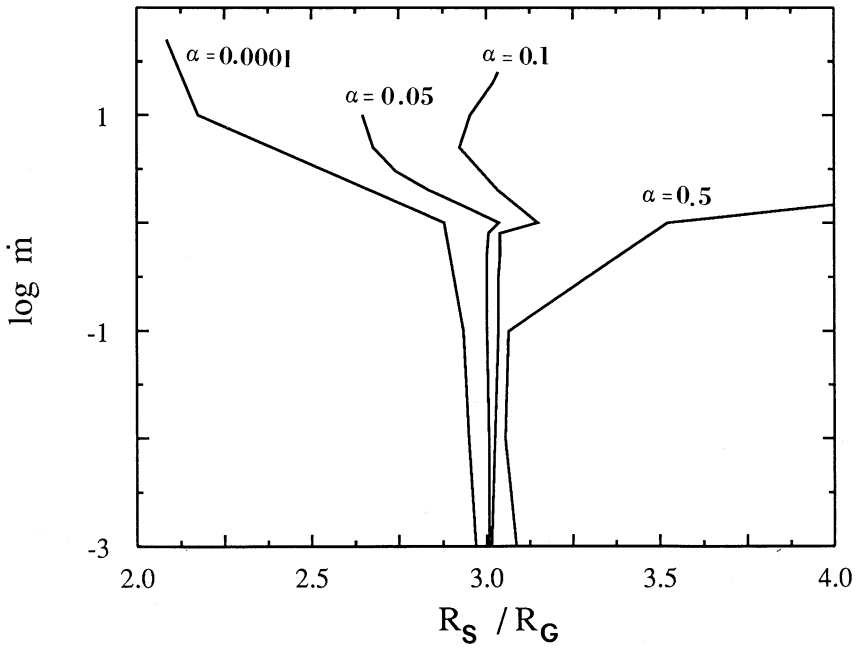

FIG. 14.—The location of the sonic point in function of the accretion rate for $\alpha = 10^{-4}$, 0.05, 0.1, and 0.5

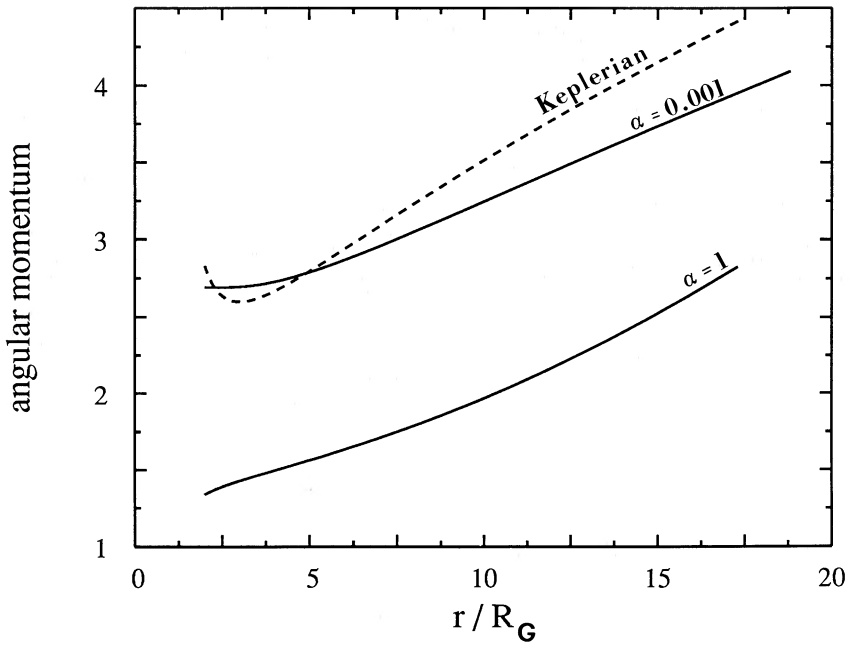

FIG. 15.—The comparison of the Keplerian angular momentum distribution (*dashed line*) with the distribution in the models with $\alpha = 0.001$ and 1 (*solid lines*), belonging to the two types of accretion.

same is true if $l(r)$ crosses the Keplerian curve, but all the crossing points are at $r > 3R_G$. Muchotrzeb-Czerny (1986) found that when the outer boundary conditions are very close to Shakura-Sunyaev ones (in the sense discussed in § III), then, which of the two different types of accretion actually occurs depends on whether α is greater or smaller than a critical value, $\alpha_{\rm crit} \approx 0.01$. She also found that in the high-viscosity case (the second type of accretion flow), the solution is not always unique. For this reason the lines on the right-hand side of Figure 14 should really be replaced by stripes. If the magnitude of the viscosity parameter, fixed in this paper to be $\alpha = 0.001$, was increased to put the models into the second regime, the whole physical picture described here would change.

b) *Different Viscosity Prescriptions*

In this paper we have used the original Shakura-Sunyaev viscosity prescription (2) which assumes that the only relevant component of the viscous stress tensor, $\tau_{r\varphi}$, is proportional to the total pressure. For strictly Keplerian accretion disks this is equivalent, with accuracy up to an irrelevant constant factor, to another phenomenological viscosity prescription

$$\nu = \alpha v_S H \,. \tag{33}$$

However, when the rotation law differs from the Keplerian one, the two viscosity prescriptions lead to physically different models. The formal reason for this is that the original Shakura-Sunyaev viscosity prescription suppresses the derivative $d\Omega/dr$, in $\tau_{r\varphi}$. Thus, with the viscosity prescription given by equation (33) there is one more differential equation in the problem. Abramowicz and Kato (1987) found that in the case of *isothermal* accretion with the viscosity prescription (2), the sonic point is either of the saddle or the nodal type, while for the viscosity law given by equation (33) only the saddle type is allowed. The different topological types of the sonic (critical) points are connected with stability and are thus physically relevant. Another widely used variation of the original Shakura-Sunyaev viscosity law assumes that $\tau_{\varphi r} = \alpha P_g$, i.e., that the viscous stress is proportional to the gas pressure rather than total pressure. It is known that in this case the $\beta < \frac{2}{5}$ instability is absent, which implies that the $\dot{M}(\Sigma)$ curves may have shapes very different from those presented here.

The viscosity coefficient α may strongly depend on the accretion rate due, for example, to the Papaloizou and Pringle (1984, 1987) instability, which for very small accretion rates may produce strong turbulence and thus viscosity, but for higher accretion rates switches off (Blaes 1987). Assume that the viscosity coefficient depends on the accretion rate through the purely phenomenological relation

$$\alpha = \alpha_0 \exp\left(-k\dot{M}/\dot{M}_C\right) . \tag{34}$$

The Shakura-Sunyaev models ($k = 0$) and their modifications ($k = 0.1, 1$) are shown in Figure 16.

Although all of the above examples indicate clearly that the exact shapes of the S-curves depend strongly on the viscosity assumption, they should not be taken as a case against the generality of the existence of the S-shaped relation $\dot{M}(\Sigma)$. In the innermost part of accretion disks around black holes (which belong to the *first type* of transonic accretion) this relation is due, as we have explained in § IV, to the relativistic Roche lobe overflow mechanism and strong advective cooling connected with it. The mechanism operates independently of viscosity. Thus, the existence of the S-shaped $\dot{M}(\Sigma)$ relation does not depend on the viscosity assumption, even if the details of particular models are very sensitive to it.

c) *The Mass of the Central Black Hole*

In this paper we consider only the case $m = 10$, which is relevant to the Galactic black holes. Physical processes discussed here do not depend on a particular value of m, however. The slim accretion disks around supermassive black holes, relevant for active galactic nuclei, will have the same general properties. The scaling from small to large masses is nonlinear, and to get the *quantitative* description of slim disks in the case of $m > 10^6$ one must repeat the calculations presented here.

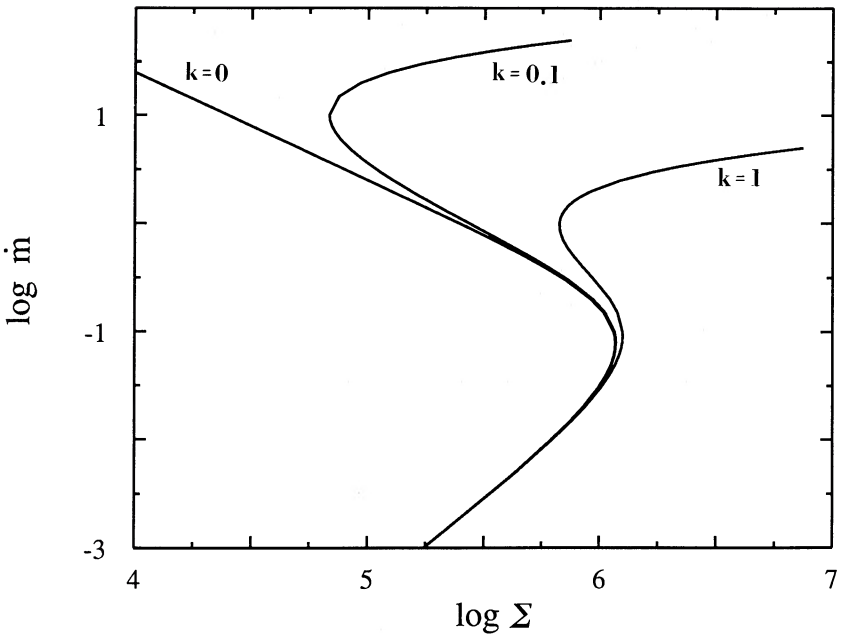

FIG. 16.—The $\dot{m}(\Sigma)$ relation for the Shakura-Sunyaev models with a modified α viscosity, given by eq. (34)

VII. CONCLUSIONS

In this paper we have discussed the role of horizontal pressure and entropy gradients in accretion disks with moderate super-Eddington accretion rates (slim accretion disks). We have found that these gradients are very important in the innermost, transonic part of the disks orbiting black holes. The most astrophysically relevant effect produced is a strong horizontal heat flux, which changes the energy balance in the disk. Due to this advective flux, the well-known $\beta < \frac{2}{5}$ instability disappears when the accretion rate is high enough. For this reason the relation between accretion rate and surface density is characteristically S-shaped. The S-shaped $\dot{M}(\Sigma)$ relation in the case of accretion disks in dwarf novae plays an important role in the explanation of the outbursts (see, e.g., Smak 1984). Similar nonstationary, quasi-periodic behavior should be expected also in the innermost, transonic part of the slim accretion disks.

We would like to thank many colleagues for help and discussion. First of all, we would like to thank D. Alloin and D. Pelat, whose observations (see Alloin *et al.* 1986) of variability of emission lines in the Seyfert galaxy NGC 1566 were the original motivation to start this theoretical work. We are also grateful to J. Frank, S. Kato, J. Krolik, M. Livio, J. Miller, B. Paczyński, S. Phinney, and D. W. Sciama for particularly helpful suggestions. M. A. and J. P. L. thank the Observatoire de Paris for support under the A.I. "Accretion et Jets." This research was also supported by the NSF grant PHY82-17853 supplemented by funds from NASA.

REFERENCES

Abramowicz, M. A. 1981, *Nature*, **294**, 235.
———. 1986, *Pub. Astr. Soc. Japan*, **294**, 235.
———. 1987, in *General Relativity and Gravitation*, ed. M. A. H. MacCallum (Cambridge: Cambridge University Press), p. 1.
Abramowicz, M. A., Calvani, M., and Nobili, L. 1980, *Ap. J.*, **242**, 772.
Abramowicz, M. A., and Kato, S. 1987, preprint.
Abramowicz, M. A., Lasota, J. P., and Xu, C. 1986, in *IAU Symposium 119, Quasars*, ed. G. Swarup and V. K. Kapahi (Dordrecht: Reidel, p. 376.
Abramowicz, M. A., and Zurek, W. H. 1981, *Ap. J.*, **246**, 314.
Alloin, D., Pelat, D., Phillips, M. M., Fosbury, R. A. E., and Freeman, K. 1986, *Ap. J.*, **308**, 23.
Begelman, M. C. 1978, *Astr. Ap.*, **70**, 583.
Begelman, M. C., Blandford, R. D., and Rees, M. J. 1984, *Rev. Mod. Phys.*, **56**, 255.
Blaes, O. M. 1987, *M.N.R.A.S.*, **227**, 975.
Cox, A. N., and Stewart, J. N. 1970, *Ap. J. Suppl.*, **19**, 243.
Jaroszyński, M., Abramowicz, M. A., and Paczyński, B. 1980, *Acta Astr.*, **30**, 1.
Kozłowski, M. Jaroszyński, M., and Abramowicz, M. A. 1978, *Astr. Ap.*, **63**, 209.
Madau, P. 1988, *Ap. J.*, **327**, 116.
Matsumoto, R., Kato, S., Fukue, J., and Okazaki, A. T. 1984, *Pub. Astr. Soc. Japan*, **36**, 71.
Muchotrzeb, B. 1983, *Acta Astr.*, **33**, 79.
Muchotrzeb-Czerny, B. 1986, *Acta Astr.*, **36**, 1.
Muchotrzeb, B., and Paczyński, B. 1982, *Acta Astr.*, **32**, 1.
Paczyński, B. 1980, *Acta Astr.*, **30**, 347.
Paczyński, B., and Bisnovatyi-Kogan, G. 1981, *Acta Astr.*, **31**, 283.
Paczyński, B., and Wiita, P. J. 1980, *Astr. Ap.*, **88**, 23.
Papaloizou, J. C. B., and Pringle, J. E. 1984, *M.N.R.A.S.*, **208**, 721.
———. 1987, *M.N.R.A.S.*, **225**, 267.
Pringle, J. E., Rees, M. J., and Pacholczyk, A. G. 1973, *Astr. Ap.*, **29**, 179.
Różyczka, M., and Muchotrzeb, B. 1982, *Acta Astr.*, **32**, 285.
Shakura, N. I., and Sunyaev, R. A. 1973, *Astr. Ap.*, **24**, 337.
Smak, J. I. 1984, *Pub. A.S.P.*, **96**, 5.
Stoeger, W. R. 1976, *Astr. Ap.*, **53**, 267.

MAREK A. ABRAMOWICZ and EWA SZUSZKIEWICZ: Scuola Internazionale di Studi Superiori Avanzati, Strada Costiera 11, 34014 Trieste, Italy

BOŻENA CZERNY: Centrum M. Kopernika Polskiej Akademii Nauk, ul. Bartycka 18, 00-716 Warszawa, Poland

JEAN PIERRE LASOTA: Groupe d'Astrophysique Relativiste CNRS, DARC, Observatoire de Paris, Section de Meudon, 95195 Meudon Principal Cedex, France